Single-Residue Solvation Perturbations Regulate Global Protein Architecture and Function

Yingya Liu[1,#], Jihang Zhai[1,#], Shanshan Cao[2], Huiying Guo[3], Hengwei Zhang[1], Bo Song[4], Jiajia Guo[3], Dong Men[2,*], Xiao He[1,5,6,7,*], Di Li[1,*]

1 School of Chemistry and Molecular Engineering, East China Normal University, Shanghai, 200241, China

2 Guangzhou National Laboratory, Guangzhou, 510005, PR China

3 Shenzhen Institutes of Advanced Technology, Chinese Academy of Sciences, Shenzhen, 518055, China

4 School of Optical-Electrical Computer Engineering, Shanghai Key Lab of Modern Optical Systems, University of Shanghai for Science and Technology, Shanghai, 200093, China

5 Shanghai Engineering Research Center of Molecular Therapeutics and New Drug Development, Shanghai Frontiers Science Center of Molecule Intelligent Syntheses, East China Normal University, Shanghai, 200062, China

6 Chongqing Key Laboratory of Precision Optics, Chongqing Institute of East China Normal University, Chongqing 401120, China

7 New York University–East China Normal University Center for Computational Chemistry, New York University Shanghai, Shanghai, 200062, China

Contents

1. Materials

Ultrapure water (18.2 MΩ·cm) was generated by Milli-Q Purification System (Millipore, USA). Anhydrous alcohol (≥ 99%), sodium chloride (NaCl, ≥ 99.9%), Dichloromethane (DCM), 1-ethyl-3-(3-(dimethylamino) propyl) carbodiimide (EDC), Dimethyl sulfoxide (DMSO) deuteroxide (D_2O), p-nitrophenyl phosphate (pNPP), 4-Methylumbelliferyl Phosphate (4-MUP), 4-Dimethylaminopyridine (DMAP), and N, N'-Dicyclohexylcarbodiimide (DCC) were purchased from Merck (USA). Tetrabutoxydisiloxane (TBDS) and Aminopropyltriethoxysilane (ATES) were obtained from United Chemical Tech. Buffer solutions, including MES, Tris, and PBS, were acquired from Biyotime Biotech. Precleaned glass microscope slides were purchased from VWR (USA). Carboxyl-functionalized spiropyran (COOH-SP) was purchased from Selectoprobe Co. Amicon Ultra-0.5 mL centrifugal filters (30 kDa MWCO; product #UFC503024) were purchased from Merck Millipore (USA). The Zeba^{TM} Spin Desalting column (7 K MWCO, 0.5 mL) and bicinchoninic acid (BCA) assay kit were purchased from Thermo Fisher Scientific.

2. Synthesis of dibenzocyclooctyne (DBCO)-functionalized SP (DBCO-SP)

2.1 Structure characterization of DBCO-SP

NMR (400 MHz, $CDCl_3$) δ (ppm)：8.10-8.09（m, 1H), 7.62-7.45 (dd, 2H), 7.42-7.29 (m, 7H), 7.07-7.05(m, 3H), 6.59-6.57(q, 1H), 6.56-6.54 (m, 3H), 5.73 (d, 1H), 5.05(d, 1H), 4.08-4.05(m, 2H), 3.61-3.34(d, 1H), 3.34-3.27(m, 2H), 2.01-2.01(m, 1H), 2.0 (t, 2H), 1.75-1.72(m, 1H), 1.36-1.13(m, 1H), 1.26(s, 6H), 1.01-0.99(d, 3H). LC-MS found (Scan ES^+): 703.63. The purity, as calculated by HPLC, is 96.65%.

2.2 Photoisomerization measurements

DBCO-SP (10 mM) was desolved in DMSO and then diluted to 0.2 mM with Tris-NaCl buffer (25 mM Tris, 100 mM NaCl, pH 7.5). Absorbance spectra were recorded on a Shimadzu UV-1800 spectrophotometer. The isomerization efficiency of the sample was evaluated by irradiating with blue light (450 nm, 10 mW/cm², LED) for different time intervals (2-20 min). The photo-responsive dynamics of DBCO-SP were evaluated by monitoring the absorbance at 540 nm after blue light illumination and dark treatments.

2.3 Contact angle measurements

Glass slides were cleaned by shaking in 1:1 (v/v) methanol/concentrated HCl for 30 min, rinsed with deionized water, and dried at 140 °C for 20 min. Dry toluene, prepared by double distillation and stored over 3 Å molecular sieves, was used to prepare TBDS and ATES solutions. Slides were incubated in TBDS solution for 30 min, rinsed with toluene, dried at 140 °C for 20 min, and then incubated in ATES solution for 30 min. After washing with toluene and water, the slides were cured at 140 °C for 30 min to 3 h. The silane-coated slides were then incubated in an ethanol solution containing SP-COOH (1 mM) and EDC (10 mM) at room temperature with gentle shaking for 30 min to 1 h. Finally, the slides were washed with ethanol and water to remove unbound SP, and dried under vacuum for 20 min[1].

The advancing contact angles on treated glass plates were measured using the sessile drop method. After illuminating the plates with appropriate light for 30 min from a distance of 2 cm, a 2 μL drop of deionized water (pH 5.5) was placed on dry regions of the plates, and images were taken within 5s. The drop was observed on a Navitar microscope equipped with a Hitachi VK-C370 digital color video camera. Images were processed with Scion Image version 1.62c to determine contact angles. The measurements were repeated for at least six dry areas per slide and across multiple slides.

3 Possible interference on the photo-regulated ALP-MC activity

The impact of solvent isotopic substitution on light-mediated enzyme was investigated by replacing H_2O with D_2O in reaction buffer (25 mM Tris, 100 mM NaCl, pD 7.4). Catalytic activity of ALP-MC was assayed under dark and blue-light illumination using pNPP and 4-MUP as substrates.

To exclude nonspecific interactions between free MC/SP isomers and ALP, enzyme-spiropyran mixtures were prepared at defined molar ratios (ALP : SP = 1:0, 1:10, 1:20, 1:50, 1:100) in reaction buffer (25 mM Tris, 100 mM NaCl, pH 7.4). Samples were incubated in the dark for 30 min at 25°C to allow MC isomerization to reach equilibrium, catalytic activity was assayed as previously described.

To eliminate potential artifacts from ALP-MC aggregation, catalytic assays were repeated in the presence of n-octyl β-D-thioglucopyranoside (OTG, Sigma-Aldrich) at 0.02% and 0.1% (w/v). OTG was added to reaction mixtures 10 min prior to substrate addition. Reactions containing 50 nM ALP-SP and 1 mM pNPP were monitored under dark and blue light-activated conditions as described in above.

4. Characterization

4.1 Fluorescence lifetime measurement

4.1.1 Instruments

Fluorescence lifetime measurements were performed using MicroTime 200 (PicoQuant, Germany) integrated with an Olympus inverted fluorescence microscope equipped with a 100×/1.45 NA oil immersion objective (UPlanApo, Olympus, Japan). A 532 nm pulsed laser (LDH-P-FA-530B, PicoQuant, Germany) operating at 40 MHz was used for excitation. The emitted fluorescence was collected through a 488/532 nm dichroic mirror (Chroma, USA) to remove scattered excitation light and further filtered using a 582/64 nm bandpass filter (Chroma, USA) to ensure spectral selectivity. Fluorescence photons were detected using a single-photon avalanche diode (SPCM-AQRH-14-TR, Excelitas, USA).

4.1.2 Sample preparation

The ALP-SP sample was incubated in the dark at room temperature for 1 h to allow full isomerization to ALP-MC. For the RMC state, sample was first illuminated with 450 nm light for 10 min to induce ring closure, and then stored in the dark at room temperature for 2 h to allow back-conversion to MC form.

4.1.3 Ensemble Measurement

Ensemble fluorescence lifetime measurements in various solvents were carried out using the MicroTime 200 in point measurement mode. For each sample, 100 μL solution (5 μM) was dropped onto a coverslip, and the laser was focused at 20 μm above the coverslip to ensure a homogeneous signal.

Fluorescence lifetime data were processed and analyzed using SymPhoTime 64 software (v2.7, PicoQuant, Germany). In the ensemble measurements, each sample

underwent testing on three concurrent replicates, with each replicate being measured three times. This approach yielded nine data points per sample, thereby ensuring both reliability and reproducibility. The resulting TCSPC decay curves were analyzed using a multi-exponential tail fitting model, and the mean value of the nine lifetimes was calculated.

The fluorescence lifetime of MC was measured in various solvents with different polarities. The calculated lifetimes did not exhibit a monotonic dependence on solvent polarity, indicating that the observed lifetime variations are governed not only by polarity but also by other factors, such as solvent viscosity[2].

4.1.4 Single-molecule measurement

The E15, K25, and V10 samples were diluted to a final concentration of 100 pM and drop-casted on a Ni^{2+}-coated coverslip at room temperature for 10 min[3, 4]. Measurements were conducted in a chamber containing 1× TAE buffer supplemented with an oxygen scavenging system (2.5 mM protocatechuic acid and 25 nM protocatechuate-3,4-dioxygenase). All single-molecule experiments were carried out at 20 °C using the MicroTime 200 system. FLIM images were acquired via galvanometric scanning, and both fluorescence lifetime and intensity data were recorded.

In single-molecule experiments, individual fluorescent spots were manually selected from the FLIM images to extract single-molecule signals for lifetime analysis. The corresponding TCSPC decay curves were fitted using a multi-exponential tail model. The lifetime histograms and total number of single-molecule events were generated by SymPhoTime 64 software. The histogram bin size was set as 400.

The single-molecule FLIM images and corresponding fluorescence lifetime decay curves revealed distinct MC lifetimes at modification sites (V10, E15, K25), highlighting the microenvironmental heterogeneity at the protein interface. The diverse trends in lifetime variation from the MC to RMC state across different modification sites suggest that local disturbances to the water network can selectively modulate the microenvironment of the hydration layer, including aspects such as hydrogen-bonding kinetics, polarity, and viscosity. The statistical analyses of the fluorescence lifetimes for

all three samples in the two states are summarized in Figure S14.

4.2 ATR-FTIR characterization of hydrated protein films

4.2.1 Preparation of hydrated protein films

ALP-MC solution was pre-concentrated to 100 mg/mL in a low ionic strength buffer (< 20 mM total ionic strength) to minimize non-volatile solutes to prevent salt crystallization during drying. For film formation, 10 μL of concentrated ALP-MC solution (100 mg/mL in 2.5 mM Tris, 10 mM NaCl, pH 7.5) was dropped onto an IR diamond window and dried under ambient humidity (30-50% relative humidity) or gentle vacuum (~3 mbar)[5]. The resulting films retained 0.1-0.15 g H_2O/g protein, corresponding to ca. ~10% water content[6, 7].

Higher hydration was controlled by adding 1 μL or 0.5 μL of Tris-NaCl buffer to the dried films, achieving final hydration levels of ca. ~100% or 50% water content (w/w). Throughout the preparation and analysis process, samples were maintained at 25°C in the dark to keep the ALP-MC state. After acquiring the spectra of ALP-MC, the sample area was sealed under a glass coverslip to keep the hydration stabilization, and then illuminated for 10 min to the ALP-SP state.

4.2.2 ATR-MIR Spectroscopy

Mid-infrared (MIR) spectroscopy was used to detect possible light-induced changes in water content. The MIR spectra measurements were carried out on a Bruker Vertex 80v FTIR spectrometer equipped with a diamond ATR crystal (MVPPro; Harrick Scientific) and mercury cadmium telluride (MCT) detector. Spectra were recorded under vacuum from 400 to 4000 cm^{-1} with 64 scans averaging at 2 cm^{-1} resolution.

Water content was quantified by the intensity ratio of a stable internal standard peak and a water-sensitive peak[8]. Here, the hydration-insensitive amide II band (~1550 cm^{-1}) from the protein backbone vibration was used as an internal standard. The O-H stretching vibration (~3500 cm^{-1}), whose intensity correlates with water content, was chosen as the hydration-sensitive peak. Their ratio (Eq. 1) normalizes protein concentration and instrumental variance, thereby extruding the changes of hydration[9].

$$R_{hyd}=\frac{I_{3500}}{I_{1500}} \quad (1)$$

The relative deviation in the hydration ratios (R_{hyd}) between ALP-MC and ALP-SP quantifies the water content variations (Eq. 2). A mean $\Delta R_{hyd} < 0.02$ g/g, below the equivalence threshold of 0.05 g/g, indicates a statistically stable hydration state.

$$\left|\frac{R_{hyd}^{SP}-R_{hyd}^{MC}}{R_{hyd}^{MC}}\right| <0.05 \quad (2)$$

4.3 Circular Dichroism (CD) Spectroscopy

The thermodynamic stabilities of ALP-MC and ALP-SP were investigated by their transition midpoint (T_m). Far-UV CD spectra were recorded from 190-300 nm on a JASCO CD spectrometer, and thermal denaturation was monitored from 20 ℃ to 95 ℃. Proteins were diluted to 50 μg/ml with buffer solution (2.5 mM Tris, 10 mM NaCl).

CD signals at characteristic α-helices (208 nm and 222 nm) were tracked continuously. Thermal denaturation profiles were generated by plotting the 208 nm signal against temperature for both proteins.

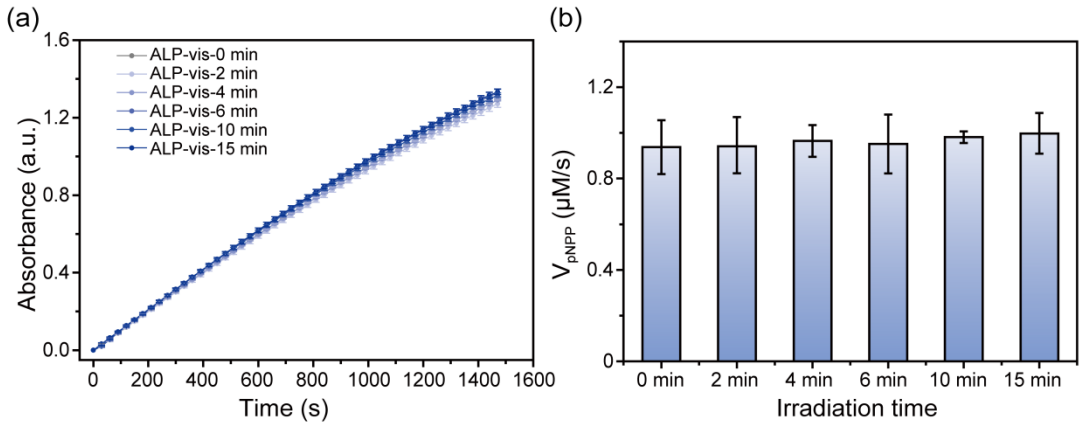

Fig. S1 Photostability of the enzymatic activity of wild-type ALP. (a) Enzymatic activity toward pNPP under 450 nm blue light illumination for indicated durations. (b) Enzymatic reaction rate toward pNPP before and after illumination for different time intervals. The data shown are presented as the mean ± SD of 3 parallel experiments.

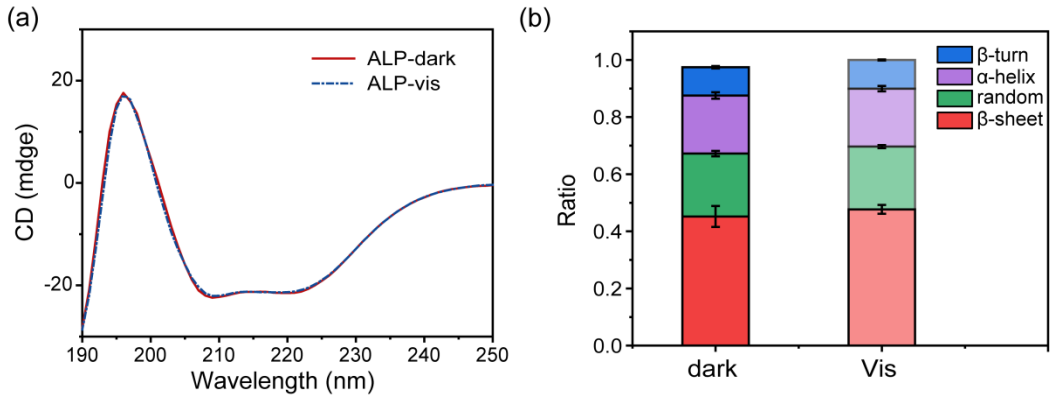

Fig. S2 Structural photostability of wild-type ALP under blue light illumination. (a) Circular dichroism (CD) spectra of ALP under 450 nm blue light (10 mW/cm²) for 10 min. (b) Secondary structure content derived from CD.

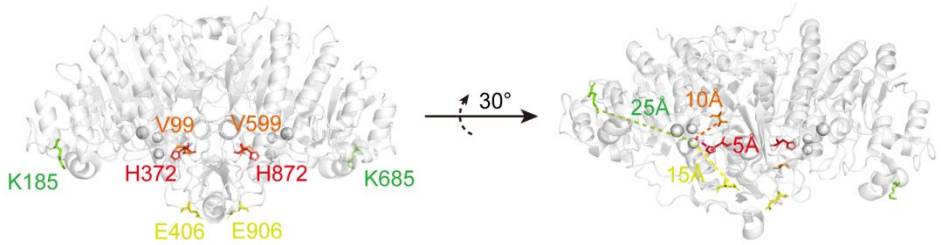

Fig. S3 Site-selective incorporation of pN_3Phe into ALP at positions H872, V599, E906, K685 (distance to catalytic center: 5→25 Å; PDB:1ED9).

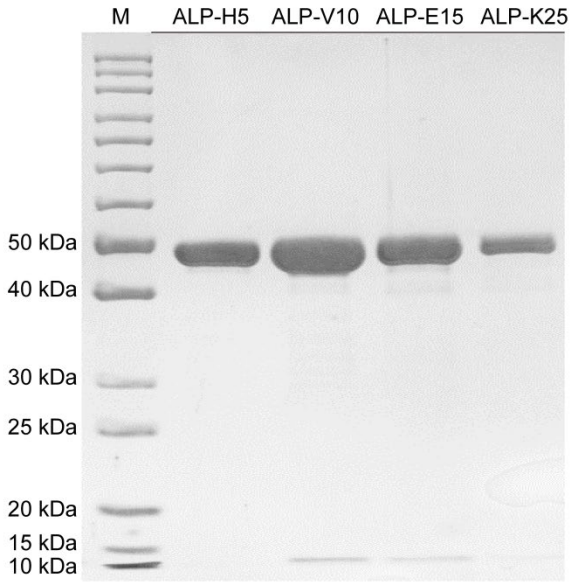

Fig. S4 Purification of Mutant ALP. SDS-PAGE (Coomassie) of H872 (H5, 5 Å), V599 (V10, 10 Å), E906 (E15, 15 Å), K685 (K25, 25 Å).

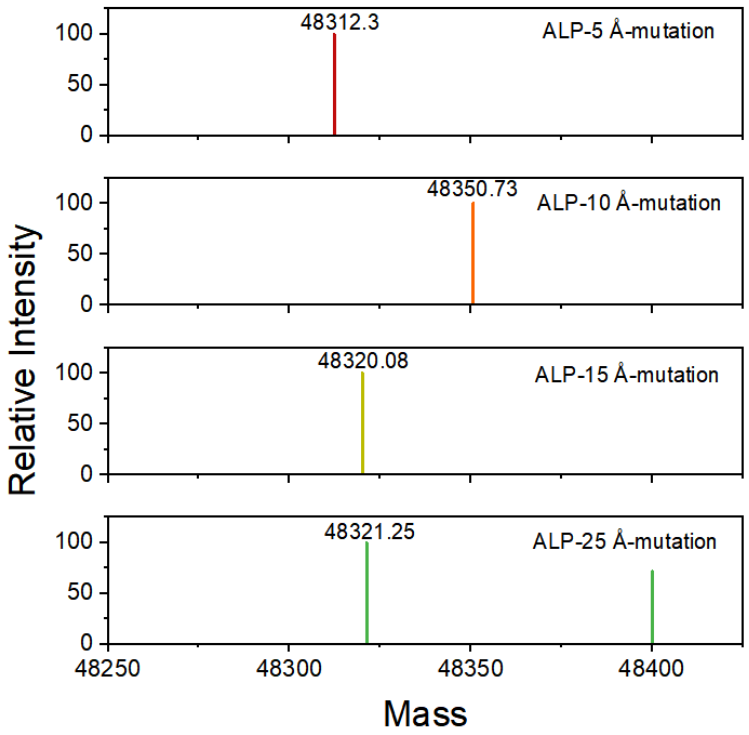

Fig. S5 LC-MS analysis of mutant ALP variants. Distance labels: H5 (5 Å), V10 (10 Å), E15 (15 Å), K25 (25 Å).

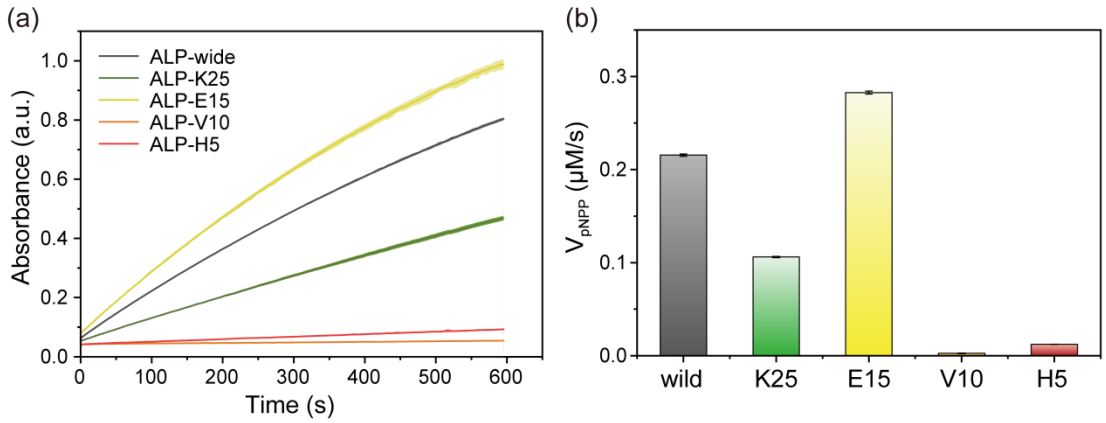

Fig. S6 Enzymatic kinetics of different ALP loop-residue mutants. (a) Time-dependent absorbance at 405 nm in pNPP hydrolysis by wild-type ALP and mutants. (b) Catalytic reaction rates of wild-type and mutant enzymes with mutants at varying distances from the active site, H5 (5 Å), V10 (10 Å), E15 (15 Å), K25 (25 Å). The data shown are presented as the mean ± SD of 3 parallel experiments.

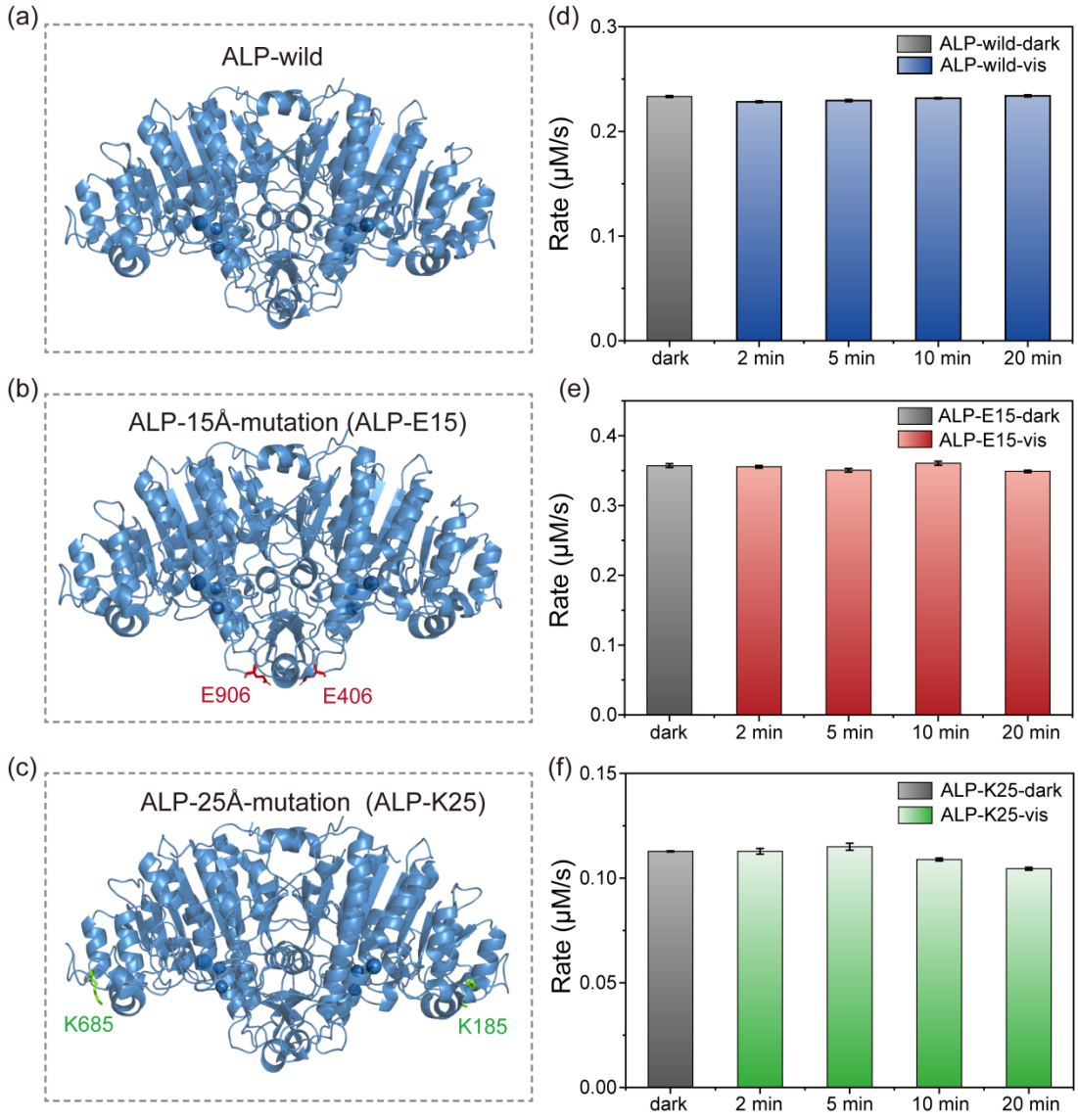

Fig. S7 Photostability of mutant ALP variants. (a-c) Structure of wild type (a), ALP-E15 (b), and ALP-K25 (c). (d-f) The enzymatic reaction rates of wild type (d), ALP-E15 (e), and ALP-K25 (f) against pNPP under blue light illumination. The data shown are presented as the mean ± SD of 3 parallel experiments.

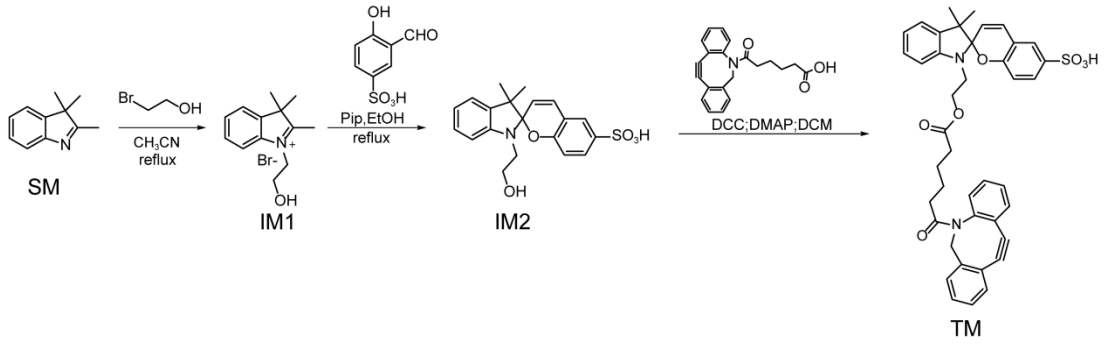

Fig. S8 Synthetic route of DBCO-SP. SM: Start material; IM: Intermediate molecule; TM: Target molecule.

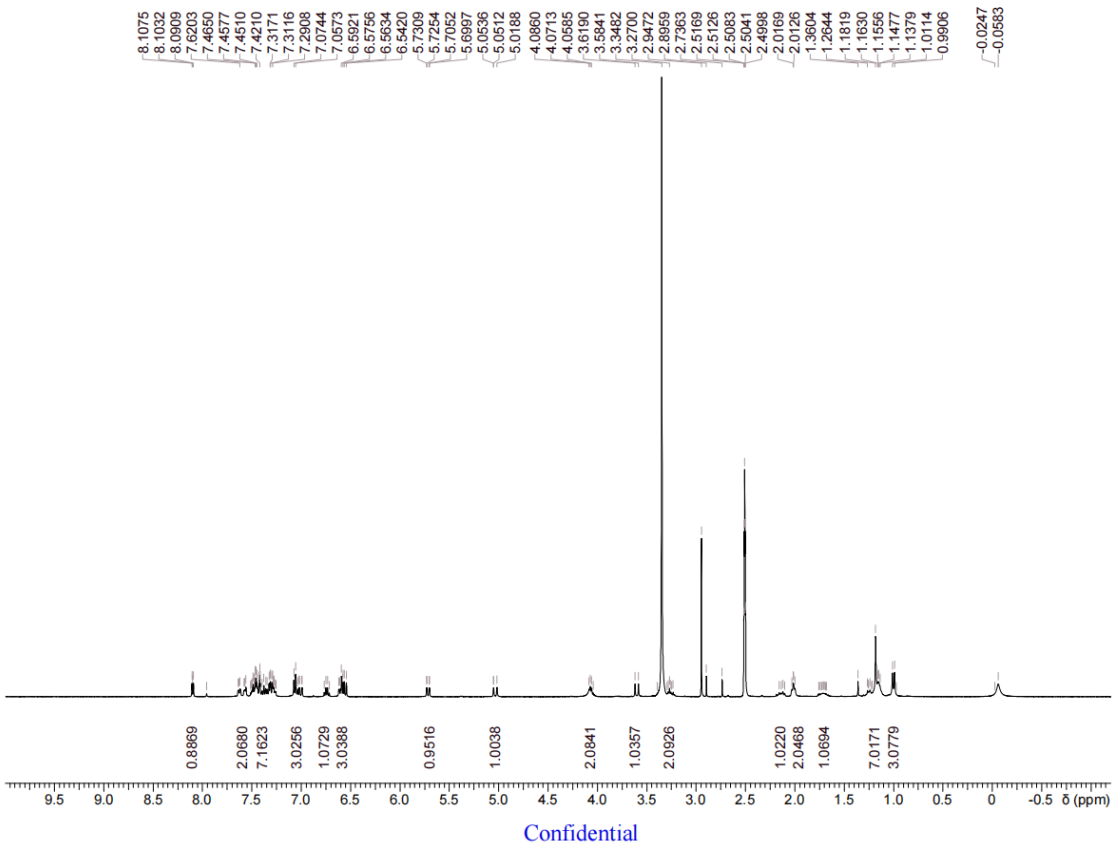

Fig. S9 ^{1}H NMR spectra of DBCO-SP in D_2O (400 MHz).

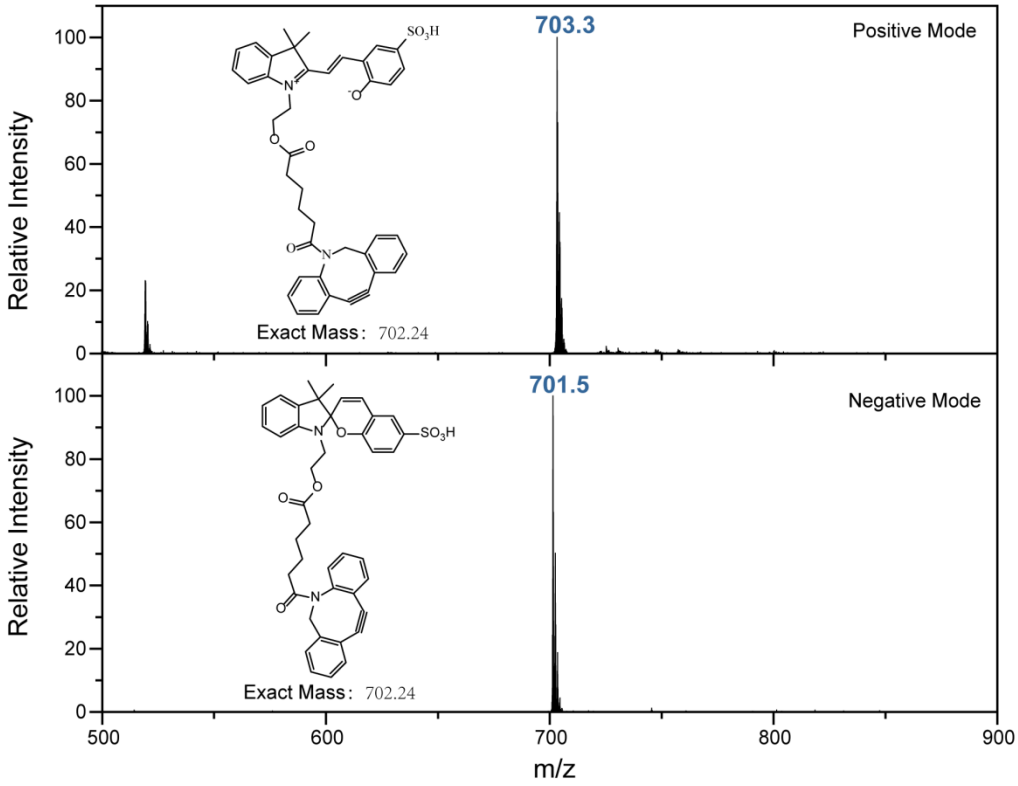

Fig. S10 UHPLC-MS spectra of DBCO-SP in positive and negative ionization modes.

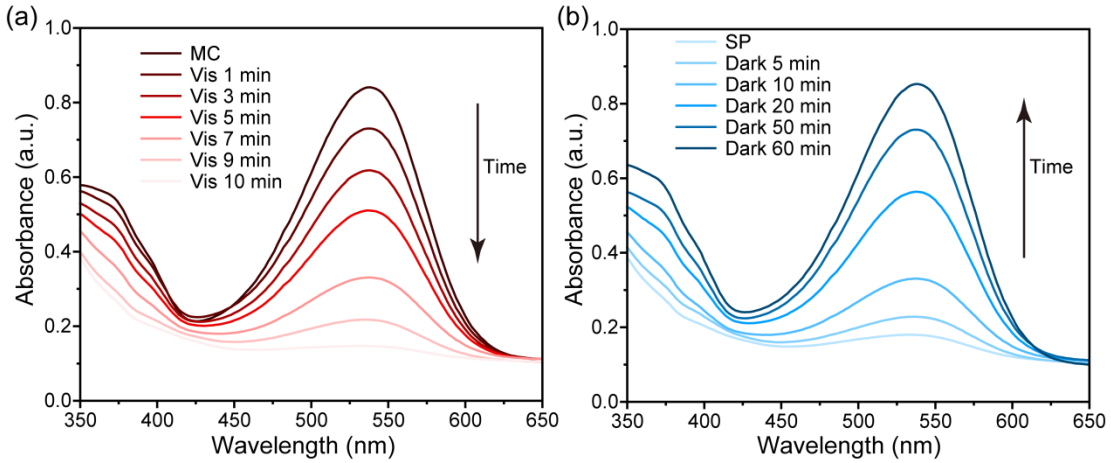

Fig. S11 Photoisomerization of DBCO-SP. (a) UV-vis spectra of DBCO-SP under blue light illumination for 1-10 min. (b) Subsequent dark recovery spectra over 60 min following cessation of illumination. All measurements were conducted at 25°C.

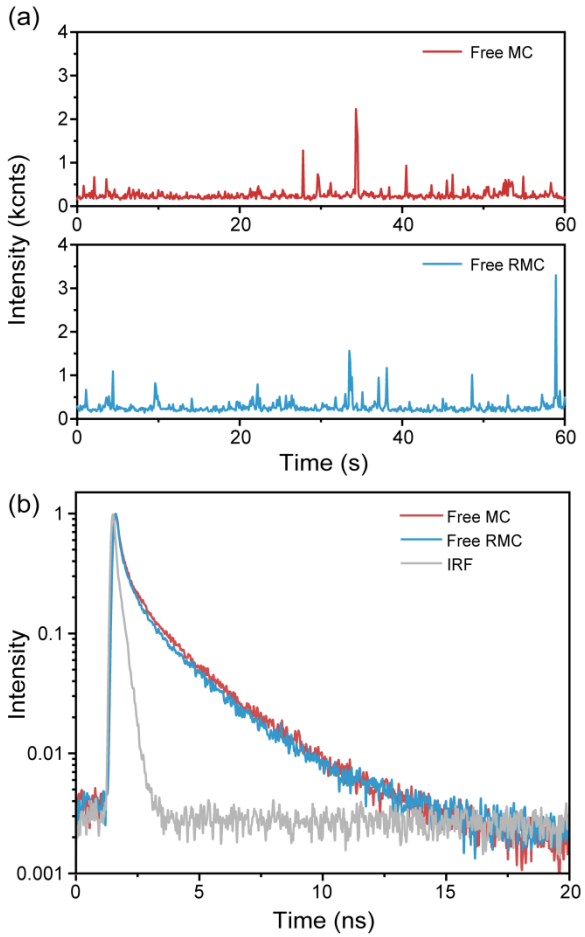

Fig. S1 Fluorescence lifetime of MC and RMC. (a) The time trace diagrams of free MC and RMC in Tris buffer. (b) Comparative analysis of fluorescence lifetimes for MC and RMC, acquired under identical experimental conditions. The instrument response function (IRF) indicates the temporal resolution.

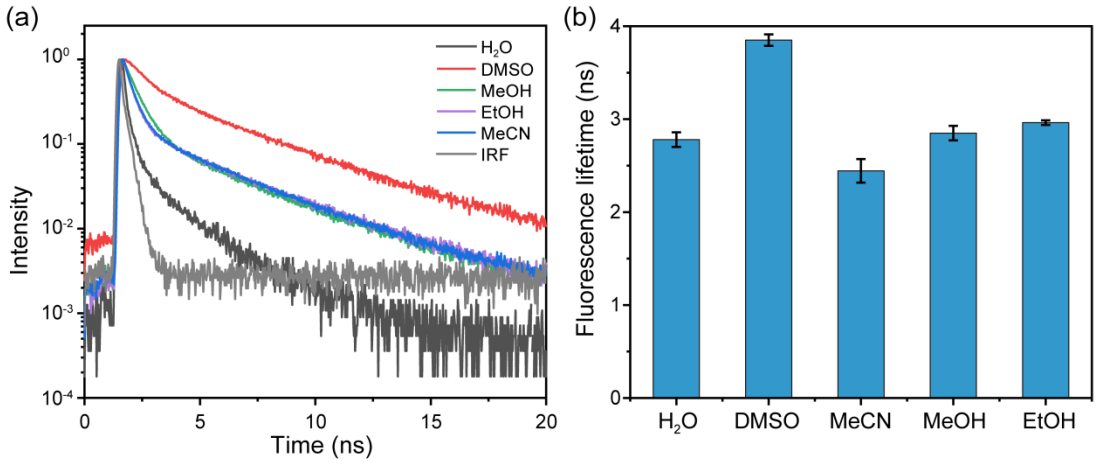

Fig. S13 TCSPC fluorescence decay kinetics of MC in different solvents. (a) Normalized decay traces of MC in H_2O, DMSO, MeCN, MeOH, and EtOH, the instrument response function (IRF) indicates the temporal resolution. (b) Comparison of the measured fluorescence lifetimes (τ) of MC across different solvents.

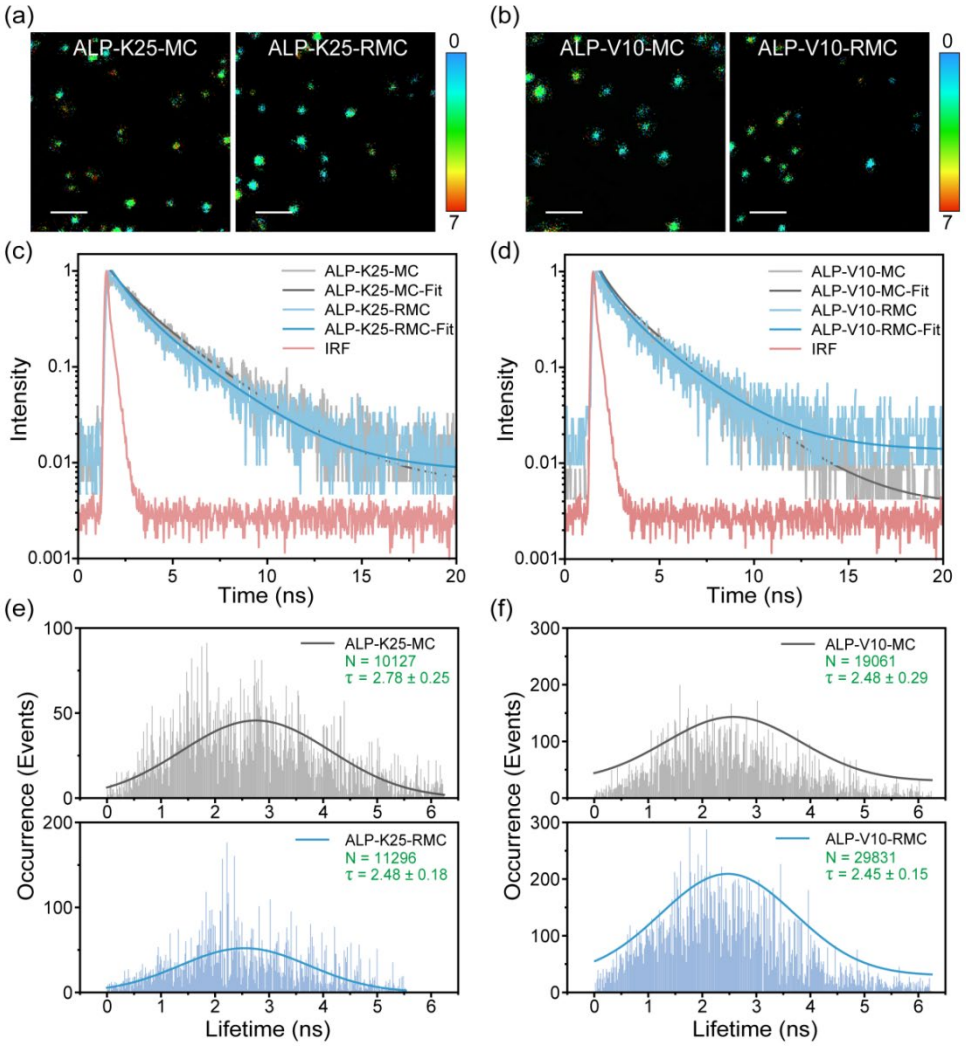

Fig. S14 Single-molecule fluorescence lifetime imaging of surface-immobilized modified-ALP variants. (a,b) Fluorescence lifetime images of (a) ALP-K25-MC/RMC and (b) ALP-V10-MC/RMC. Scale bar: 2 μm. Color scale represents lifetime values (right). (c,d) Ensemble-averaged TCSPC decay curves for (c) ALP-K25-MC and -RMC, (d) ALP-V10-MC and -RMC. (e,f) Corresponding lifetime histograms with Gaussian fits for (e) K25 variants, (f) V10 variants. Mean lifetime (τ ± σ) and molecule count (N) annotated.

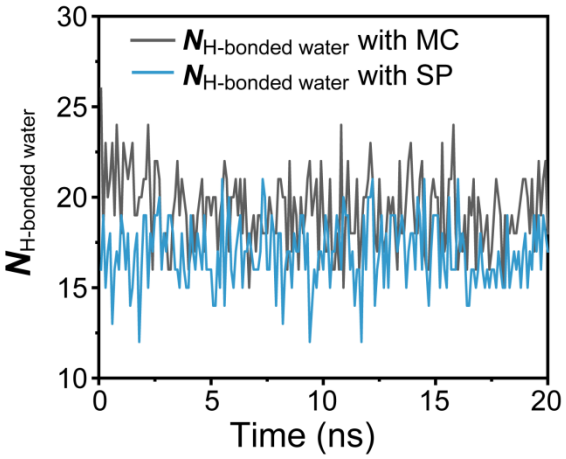

Fig. S15 The number of H-bound water molecules around the modified MC and SP site.

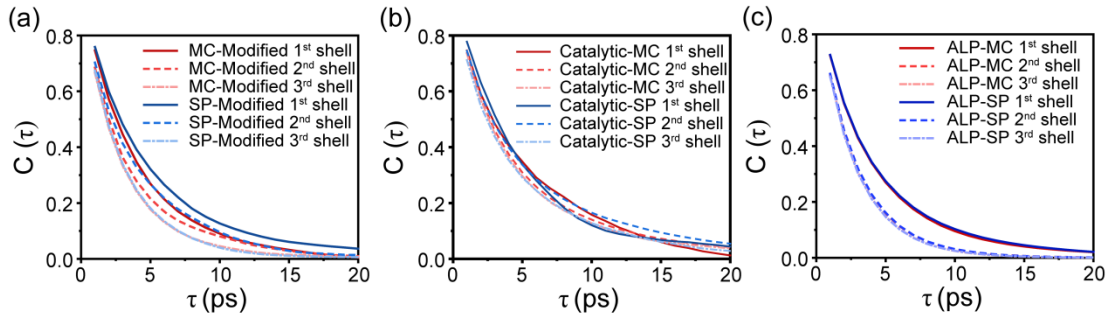

Fig. S16 Spatially resolved hydration dynamics at the interface of ALP-MC *vs* ALP-SP. Water-water (w-w) hydrogen bond (HB) self-correlation functions within distinct hydration shells (1st, 2nd, and 3rd layers) at (a) modified site, (b) catalytic site, and (c) global protein. These data characterized layer-specific hydrogen bond dynamics in the hydration environments surrounding ALP-MC and ALP-SP.

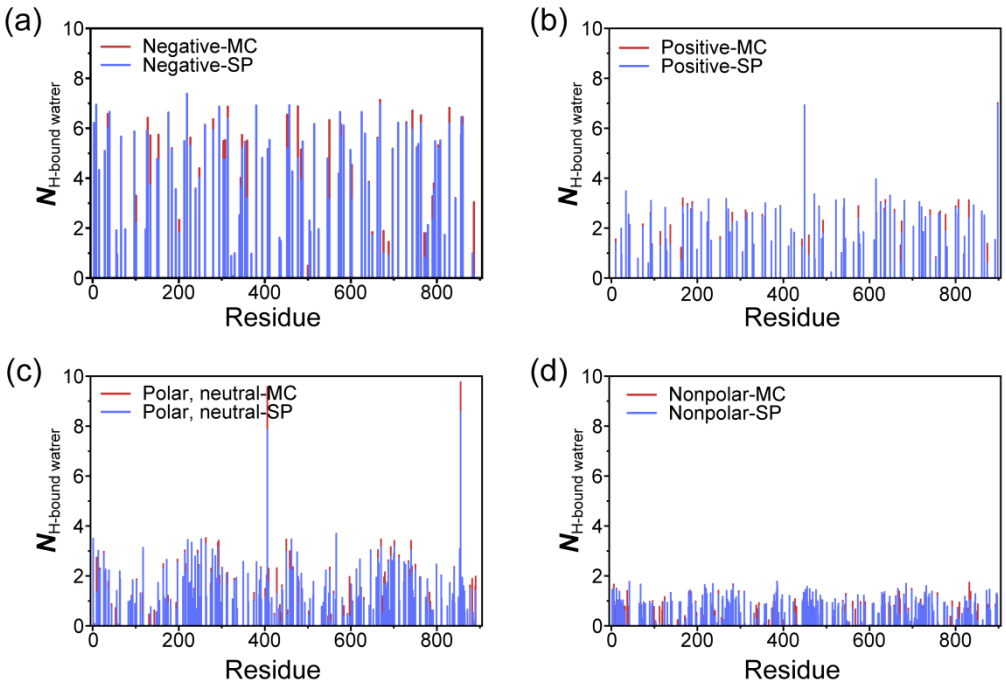

Fig. S17 The number of H-bonded water molecules ($N_{\text{H-bound water}}$) per residue type in ALP-MC and ALP-SP. (a) negatively charged residues, (b) positively charged residues, (c) polar (neutral) residues, (d) nonpolar residues.

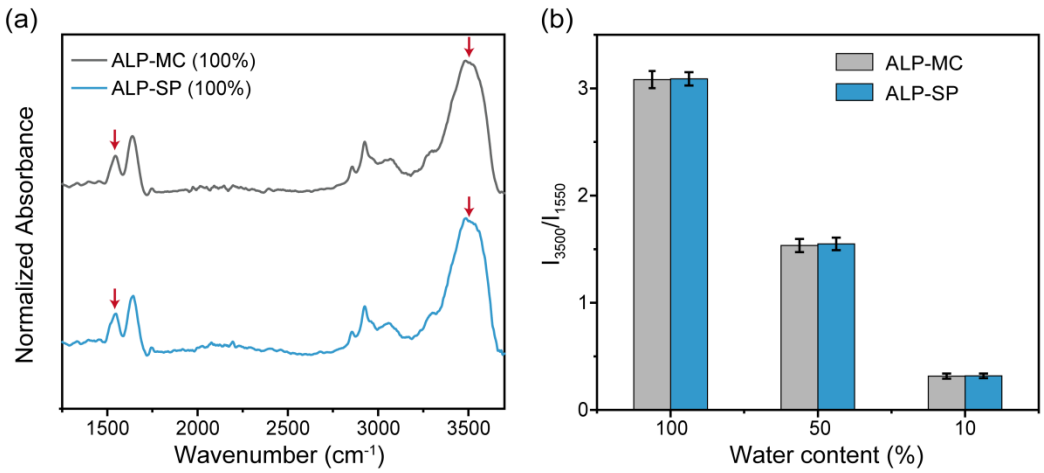

Fig. S18 The Effect of illumination on the changes water content of hydrated protein film. (a) FTIR spectra of hydrated protein films after photoisomerization. Red arrows denote the O-H stretching band of water (~3500 cm^{-1}) and amide II band (~1550cm^{-1}). (b) Relative water content (normalized to amide II) for ALP-MC and ALP-SP across hydration levels (10-100%). The data shown are presented as the mean ± SD of 3 parallel experiments.

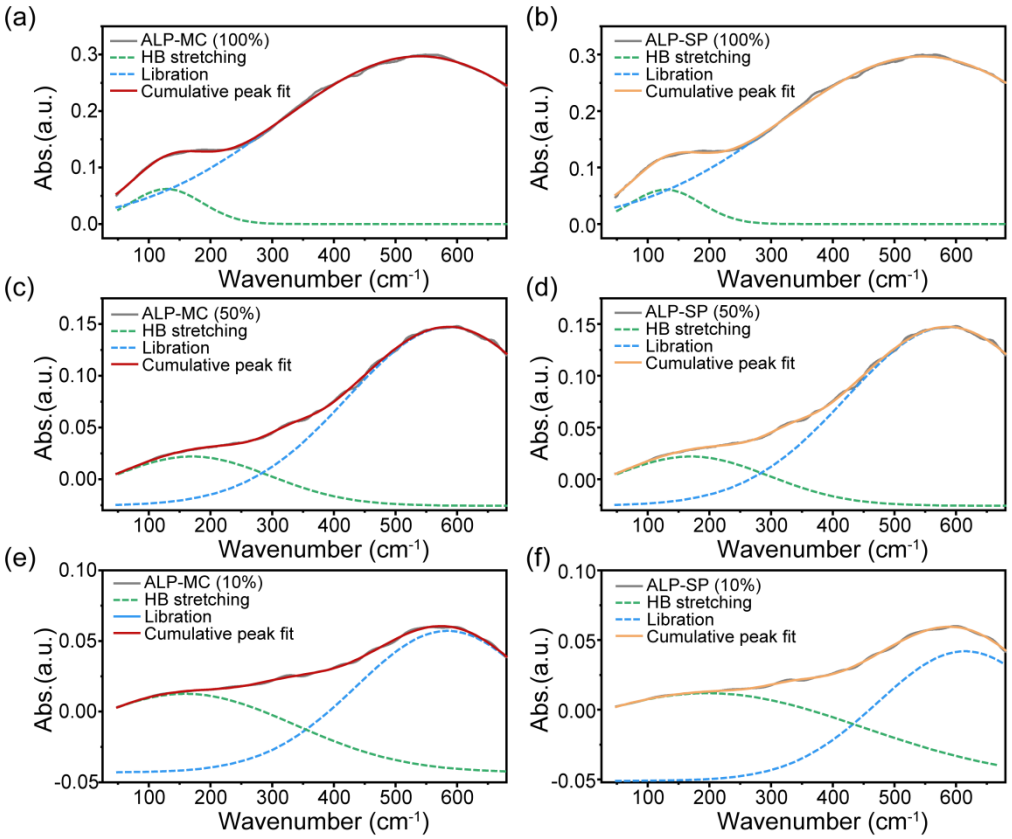

Fig. S19 Fitted THz peak frequencies (ν_{HB}, ν_{Lib}) for ALP-MC and ALP-SP under different hydration levels. (a, b) 100% hydration, (c, d) 50% hydration, (e, f) 10% hydration.

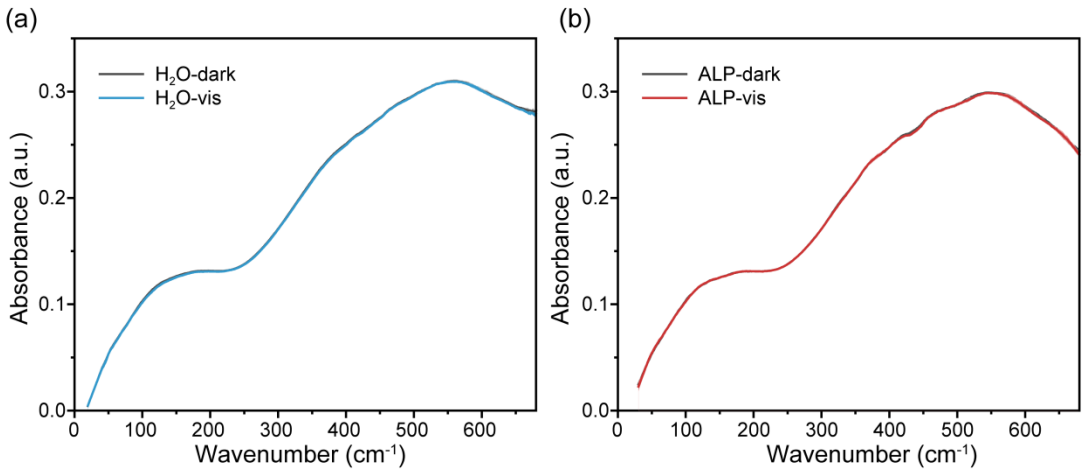

Fig. S20 The Effect of illumination on THz absorbance spectra. Spectra changes of (a) pure water and (b) unmodified ALP after exposure to 450 nm light for 10 min.

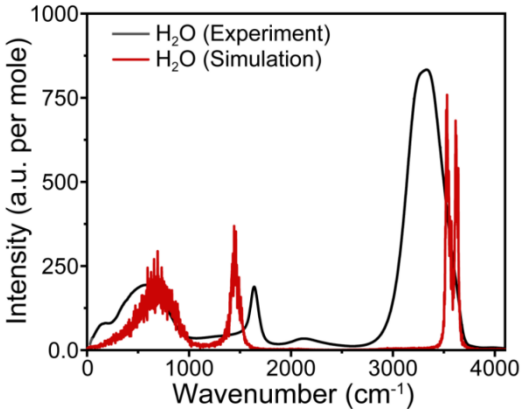

Fig. S21 Comparison of the full MD calculated IR spectrum with standard experimental H_2O data.

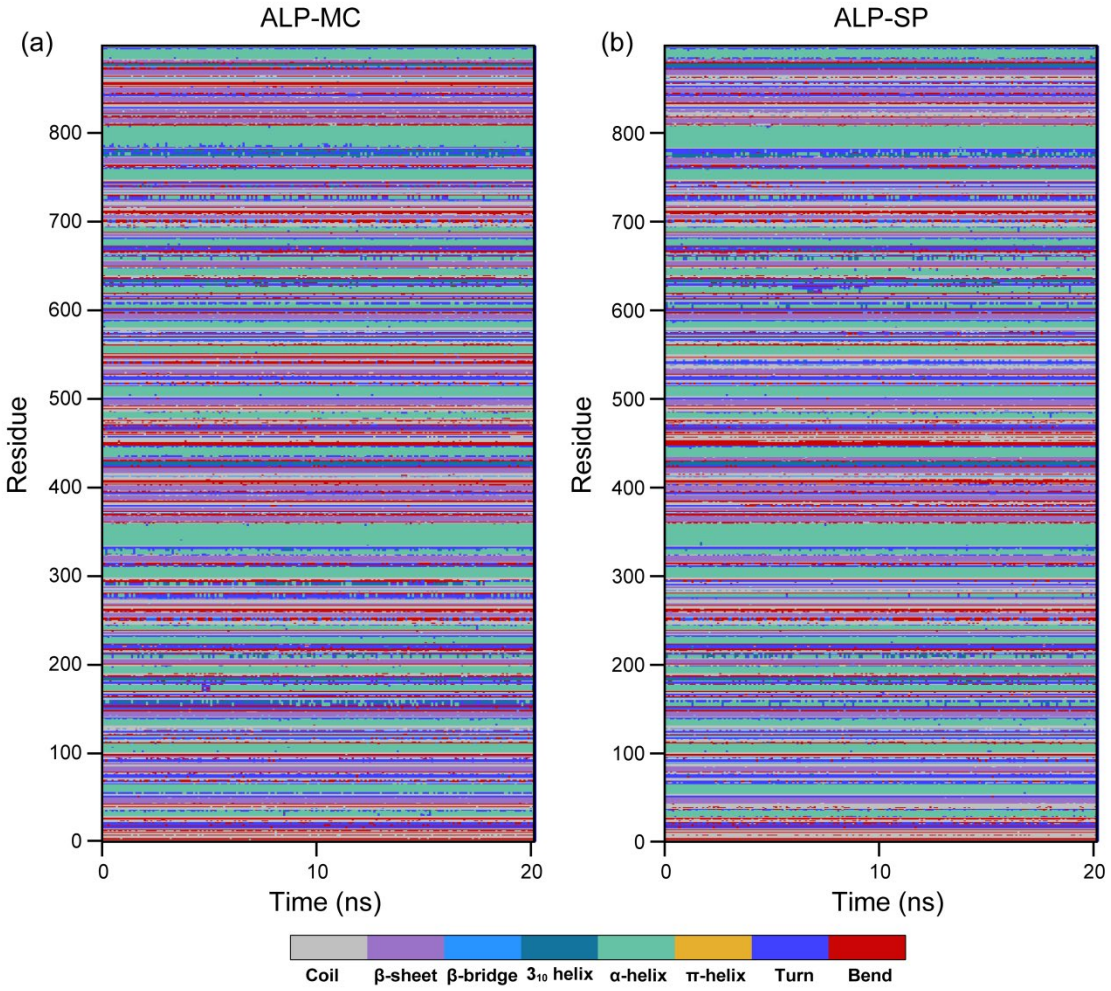

Fig. S22 Definition of Secondary Structure of Proteins (DSSP) analysis of all residues (480-500 ns). (a) ALP-MC, (b) ALP-SP. Secondary structure distribution: coil (loop), β-sheet (extended, bridge), helix (3_{10}, α, π), and turn (turn, bend).

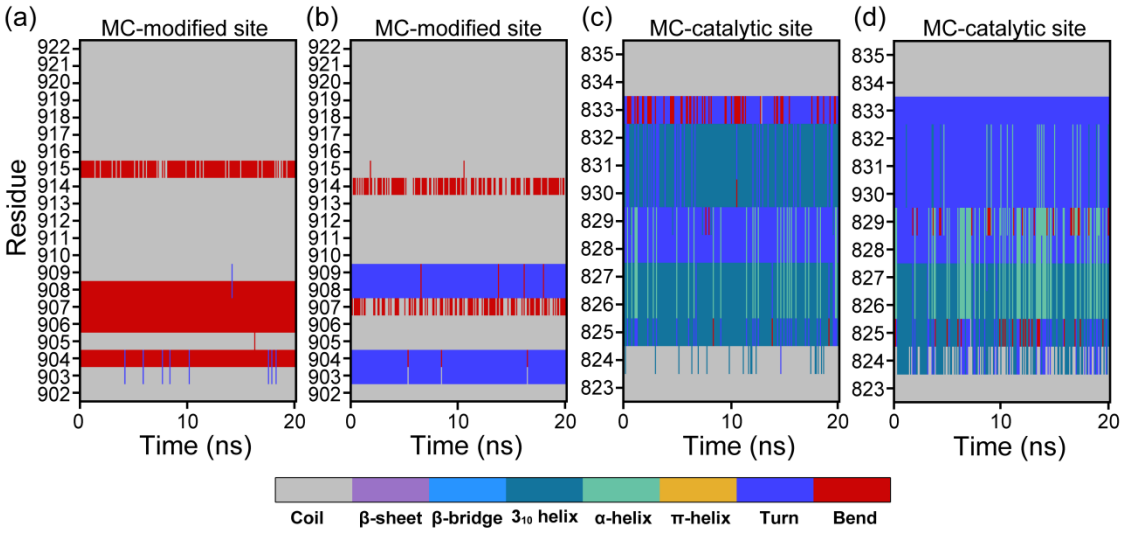

Fig. S23 DSSP analysis of ALP-MC and ALP-SP (480-500 ns). (a,b) Residues 902-922 (modified site), (c,d) Residues 823-835 (catalytic site). Secondary structure distribution: coil (loop), β-sheet (extended, bridge), helix (3_{10}, α, π), and turn (turn, bend).

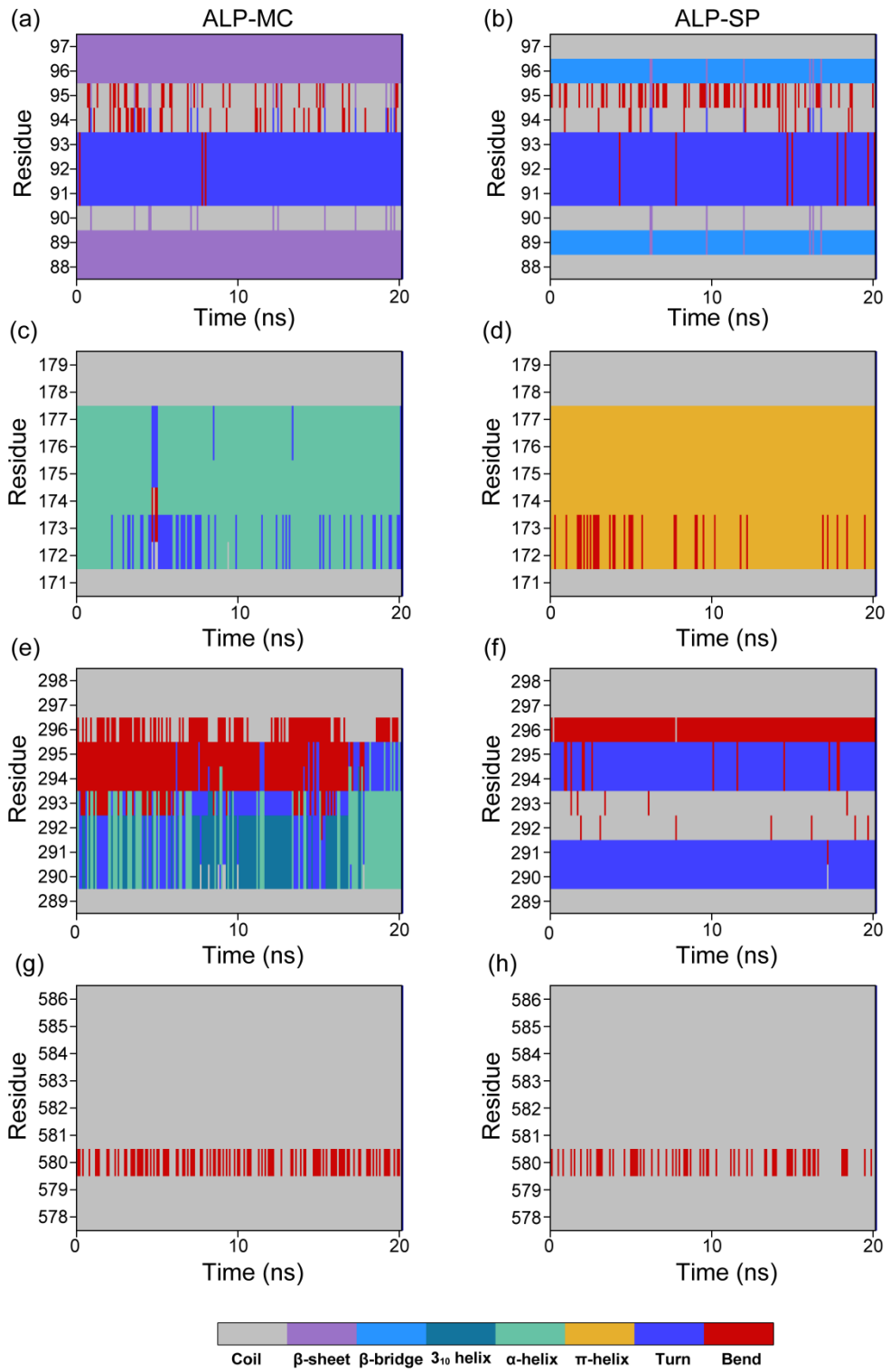

Fig. S24 DSSP analysis of different residues from ALP-MC and ALP-SP (480-500 ns). (a, b) Residues 88-97. (c, d) Residues 171-179. (e, f) Residues 289-298. (g, h) Residues 578-586. Secondary structure distribution: coil (loop), β-sheet (extended, bridge), helix (3_{10}, α, π), and turn (turn, bend).

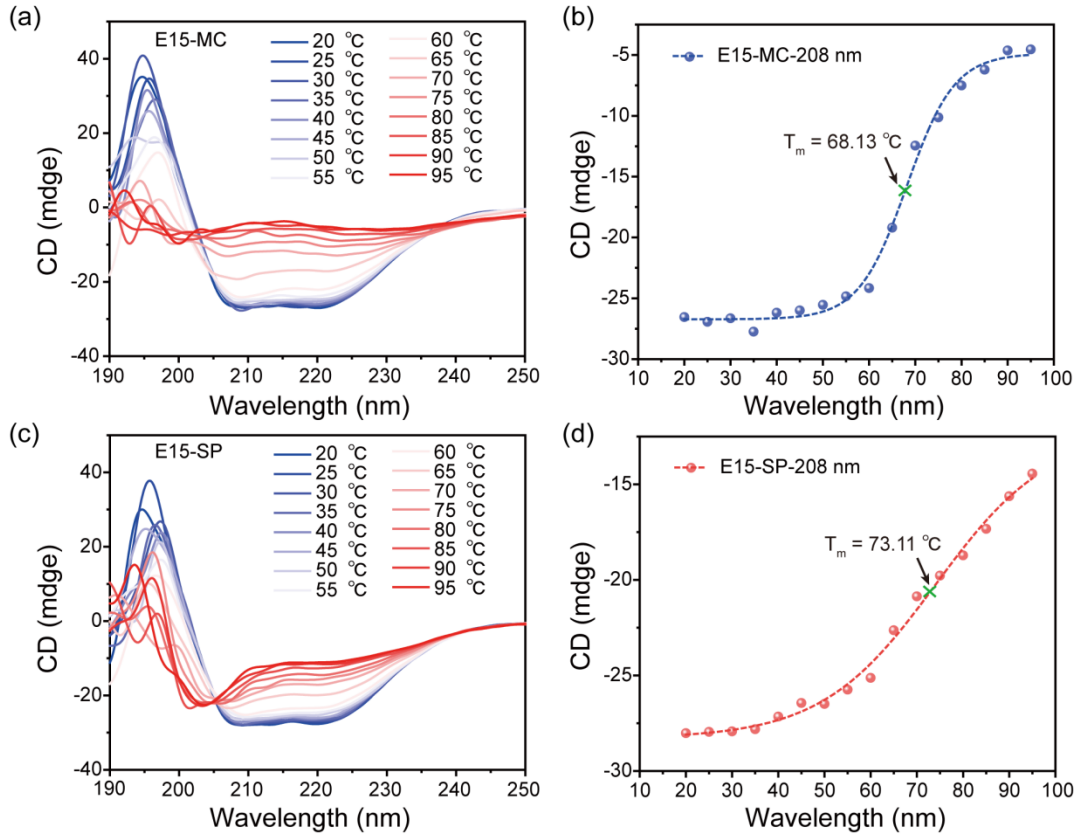

Fig. S25 Thermal stability of ALP-MC and ALP-SP. (a,c) CD spectra of ALP-MC and ALP-SP as a function of temperature from 5 ℃ to 90 ℃. (b, d) Plots of CD intensity at 208 nm versus temperature.

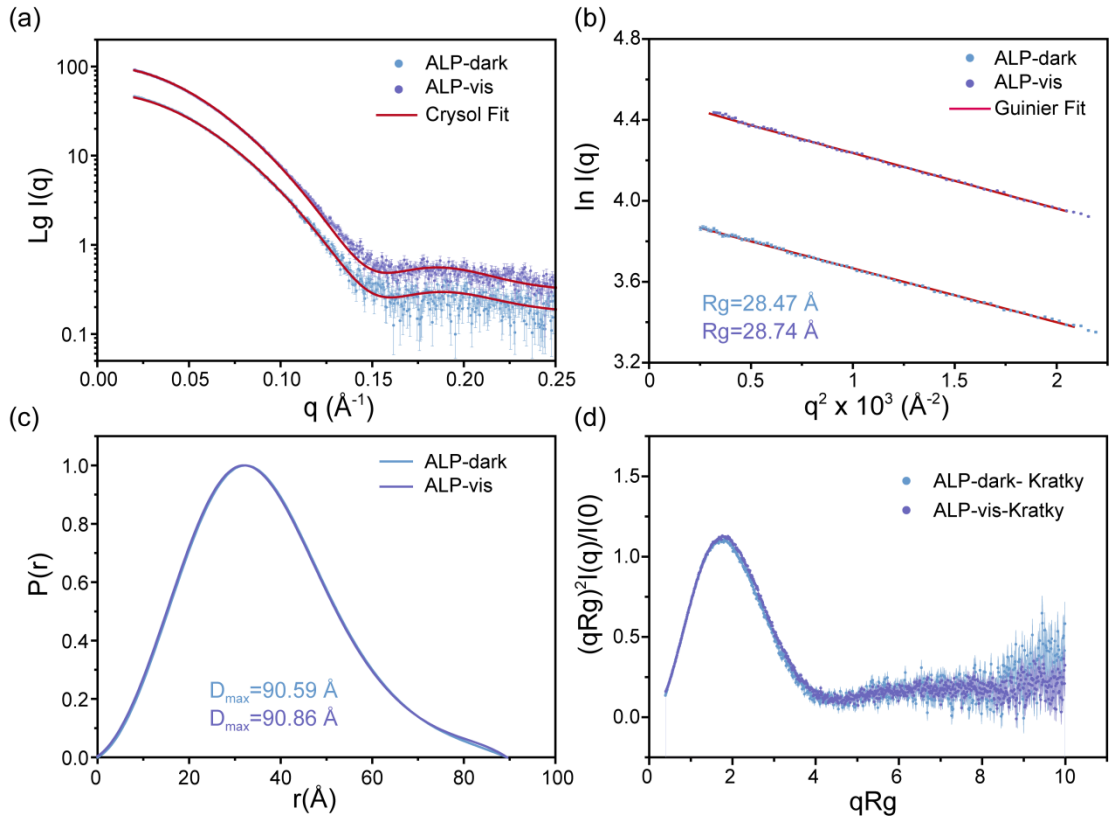

Fig. S26 SAXS analysis of light-induced structural dynamics of ALP. (a) SAXS scattering profiles (plotted as log I(q) vs q, where $q = 4\pi\sin\theta/\lambda$) for ALP-dark and ALP-vis. (b) Linear regions of Guinier plots for ALP-dark and ALP-vis, from which Rg and I(0) were derived. (c) Distance probability functions p(r) of the two samples. (d) Dimensionless Kratky plots of scattering curves for the two samples ($(qRg)^2I(q)/I(0)$ vs. qRg).

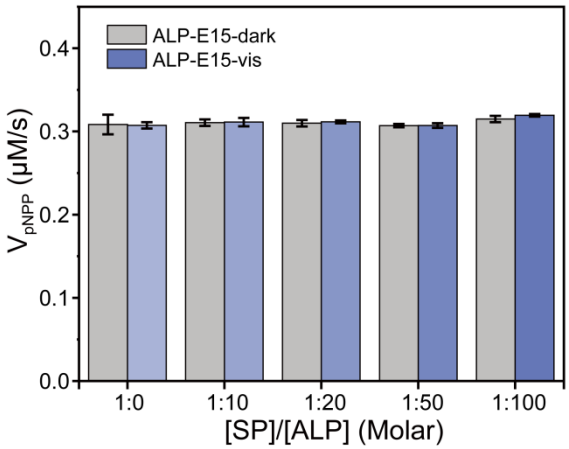

Fig. S27 Light-modulated activity of ALP/SP mixture. Enzymatic rate toward pNPP after blue light illumination. The data shown are presented as the mean ± SD of 3 parallel experiments.

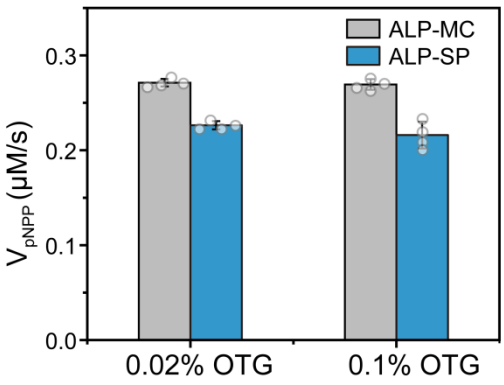

Fig. S28 Effects of detergent octylthioglucoside (OTG, 0.02-0.1% w/v) on the light-modulated ALP activity. The data shown are presented as the mean ± SD of 4 parallel experiments.

References

(1) Rosario, R.; Gust, D.; Hayes, M.; Jahnke, F.; Springer, J.; Garcia, A. A. Photon-modulated wettability changes on spiropyran-coated surfaces. *Langmuir* **2002**, *18* (21), 8062-8069.
(2) Ma, J. B.; Sun, R.; Xia, K. F.; Xia, Q. X.; Liu, Y.; Zhang, X. Design and application of fluorescent probes to detect cellular physical microenvironments. *Chem Rev* **2024**, *124* (4), 1738-1861.
(3) Kang, E.; Park, J. W.; McClellan, S. J.; Kim, J. M.; Holland, D. P.; Lee, G. U.; Franses, E. I.; Park, K.; Thompson, D. H. Specific adsorption of histidine-tagged proteins on silica surfaces modified with ni
/nta-derivatized poly(ethylene glycol). *Langmuir* **2007**, *23* (11), 6281-6288.
(4) Cha, T.; Guo, A.; Zhu, X. Y. Enzymatic activity on a chip: The critical role of protein orientation. *Proteomics* **2005**, *5* (2), 416-419.
(5) Li, P. F.; Merz, K. M. Taking into account the ion-induced dipole interaction in the nonbonded model of ions. *J Chem Theory Comput* **2014**, *10* (1), 289-297.
(6) Goormaghtigh, E.; Raussens, V.; Ruysschaert, J. M. Attenuated total reflection infrared spectroscopy of proteins and lipids in biological membranes. *Bba-Rev Biomembranes* **1999**, *1422* (2), 105-185.
(7) Lórenz, V. A.; Villaverde, J.; Trézéguet, V.; Lauquin, G. J. M.; Brandolin, G.; Padrós, E. The secondary structure of the inhibited mitochondrial adp/atp transporter from yeast analyzed by ftir spectroscopy. *Biochemistry-Us* **2001**, *40* (30), 8821-8833.
(8) Noguchi, T.; Sugiura, M. Flash-induced ftir difference spectra of the water oxidizing complex in moderately hydrated photosystem ii core films: Effect of hydration extent on s-state transitions. *Biochemistry-Us* **2002**, *41* (7), 2322-2330.
(9) Polander, B. C.; Barry, B. A. Detection of an intermediary, protonated water cluster in photosynthetic oxygen evolution. *P Natl Acad Sci USA* **2013**, *110* (26), 10634-10639.